Redox-Dependent Magnetic Alignment of *Clostridium pasteurianum* Rubredoxin: Measurement of Magnetic Susceptibility Anisotropy and Prediction of Pseudocontact Shift Contributions

Brian F. Volkman,[†] Steven J. Wilkens,[‡] Andrew L. Lee,[§] Bin Xia,[†,||] William M. Westler,[†] Richard Beger,[⊥] and John L. Markley*[,†]

Contribution from the National Magnetic Resonance Facility at Madison, Department of Biochemistry, and Graduate Program in Biophysics, University of Wisconsin−Madison, 433 Babcock Drive, Madison, Wisconsin 53706, Department of Biochemistry and Biophysics, University of Pennsylvania School of Medicine, Philadelphia, Pennsylvania 19104-6059, and National Center for Toxicological Research, Jefferson, Arkansas 72079

Received January 5, 1999. Revised Manuscript Received March 18, 1999

Abstract: An analysis of the magnetic field dependence of one-bond couplings has yielded the magnetic susceptibility anisotropies for *Clostridium pasteurianum* rubredoxin (Rdx) in its oxidized Fe(III) and reduced Fe(II) states. Experimental one-bond $^1H^N-^{15}N$ and $^1H^\alpha-^{13}C^\alpha$ couplings were measured at two field strengths (corresponding to 400 and 750 MHz ^1H frequencies) and decomposed into their field-independent scalar (^1J) and field-dependent dipolar (^1D) components. The total numbers of measured dipolar couplings ($^1H^N-^{15}N$ plus $^1H^\alpha-^{13}C^\alpha$) were 50 for oxidized Rdx and 49 for reduced Rdx. The atom pairs giving rise to these signals are located >11 Å from the iron; those closer to the iron are too broad to be resolved in two-dimensional NMR spectra and may exhibit large Fermi contact shifts. A five-dimensional grid search and Powell minimization of the difference between each set of measured dipolar couplings and those calculated from an X-ray crystal structure of Fe(III) Rdx yielded the magnitude and orientation of the magnetic susceptibility anisotropy in each oxidation state. (The data for Fe(II) Rdx were analyzed in terms of the X-ray structure for Fe(III) Rdx because no X-ray coordinates were available for the reduced rubredoxin. The assumption underlying this approximation, that the conformations of the oxidized and reduced rubredoxin are very similar in protein regions >11 Å from the iron, was validated by comparisons of experimental and calculated pseudocontact shifts.) The axial and rhombic magnetic susceptibility anisotropies were 5.3×10^{-28} and 2.1×10^{-28} cm^3/molecule, respectively, for oxidized Rdx, and 20.3×10^{-28} and 9.7×10^{-28} cm^3/molecule, respectively, for reduced Rdx. The derived susceptibility tensors were then used to calculate the pseudocontact contributions to the backbone $^1H^\alpha$ and $^1H^N$ chemical shifts of Rdx in the two oxidation states. Oxidation-state-dependent pseudocontact shifts were found to account fully (within experimental error) for the experimental chemical shift differences exhibited by these backbone signals. Thus, the results are consistent with the absence of appreciable conformational differences between Fe(III) Rdx and Fe(II) Rdx in the protein regions represented by the NMR data (>11 Å from the iron).

Introduction

Rubredoxins represent the simplest type of iron−sulfur proteins, in that they contain a single iron ion ligated by sulfur atoms from a surrounding cage of four cysteine residues. These small proteins are strongly paramagnetic in both accessible oxidation states. Both oxidized rubredoxin ($S = {}^5/_2$) and reduced rubredoxin ($S = 2$) adopt high-spin electronic configurations. The rubredoxin from *Clostridium pasteurianum* (Rdx), molecular weight 6100,[1] is one of the best-studied members of this family. The X-ray crystal structure of Fe(III) Rdx has been solved and refined to a resolution of 1.1 Å.[2−4]

Rdx has been expressed in *Escherichia coli*,[5] and we have recently developed efficient biosynthetic methods for labeling Rdx uniformly and selectively with stable isotopes for NMR investigations.[6] Using these labeled samples, we have assigned ^1H, ^2H, ^{13}C, and ^{15}N signals in both the diamagnetic[7,8] and paramagnetic spectral regions.[9] The chemical shifts of amide nitrogens that hydrogen bond to cysteine sulfur atoms ligated

* To whom correspondence should be addressed. E-mail: markley@nmrfam.wisc.edu. Phone: 608-262-3173. Fax: 608-262-3759.
[†] Department of Biochemistry, University of Wisconsin−Madison.
[‡] Graduate Program in Biophysics, University of Wisconsin−Madison.
[§] University of Pennsylvania School of Medicine.
[⊥] National Center for Toxicological Research.
[||] Current address: The Scripps Research Institute, La Jolla, CA.

(1) Petillot, Y.; Forest, E.; Mathieu, I.; Meyer, J. P.; Moulis, J.-M. *Biochem. J.* **1993**, *296*, 657−661.
(2) Watenpaugh, K. D.; Sieker, L. C.; Jensen, L. H. *J. Mol. Biol.* **1979**, *131*, 509−522.
(3) Watenpaugh, K. D.; Sieker, L. C.; Jensen, L. H. *J. Mol. Biol.* **1980**, *138*, 615−633.
(4) Dauter, Z.; Wilson, K. S.; Sieker, L. C.; Moulis, J.-M.; Meyer, J. P. *Proc. Natl. Acad. Sci. U.S.A.* **1996**, *93*, 8836−8840.
(5) Mathieu, I.; Meyer, J. P.; Moulis, J.-M. *Biochem. J.* **1992**, *285*, 255−262.
(6) Xia, B.; Westler, W. M.; Cheng, H.; Meyer, J. P.; Moulis, J.-M.; Markley, J. L. *J. Am. Chem. Soc.* **1995**, *117*, 5347−5350.
(7) Volkman, B. F.; Prantner, A. M.; Wilkens, S. J.; Xia, B.; Markley, J. L. *J. Biomol. NMR* **1997**, *10*, 409−410.
(8) Prantner, A. M.; Volkman, B. F.; Wilkens, S. J.; Xia, B.; Markley, J. L. *J. Biomol. NMR* **1997**, *10*, 411−412.
(9) Wilkens, S. J.; Xia, B.; Weinhold, F.; Markley, J. L.; Westler, W. M. *J. Am. Chem. Soc.* **1998**, *120*, 4806−4814.

10.1021/ja990079b CCC: $18.00
Published on Web 04/24/1999

to the iron have been shown to exhibit large one-bond isotope effects transmitted through the hydrogen bond.[6,10] In addition, relaxation rates of the backbone ^{15}N signals of Rdx have been measured in both oxidation states.[11] The large ^{1}H, ^{2}H, ^{13}C, and ^{15}N hyperfine shifts dominated by Fermi contact interactions,[9] the isotope effects on ^{15}N shifts,[10] and the deviations of relaxation rates from a pure dipole−dipole model[11] have all been modeled successfully by hybrid density functional analysis of a 104-atom fragment of Rdx derived from the X-ray structure. However, the sizable chemical shift differences between signals in the diamagnetic regions of Fe(II) Rdx and Fe(III) Rdx[7,8] remained unanalyzed. These sharp peaks with oxidation-state-dependent chemical shifts are assigned to nuclei located >11 Å from the iron. The chemical shift differences could arise from conformational differences in the oxidized and reduced protein or from electron−nuclear dipole−dipole interactions (pseudocontact shifts).

It has been reported that the differences between the X-ray structures of Fe(III) Rdx and Fe(II) Rdx are small, although the coordinates for the reduced protein have not yet been released.[4] Coordinates are available, however, for the oxidized and reduced forms of the thermostable rubredoxin from *Pyrococcus furiosus*; in this rubredoxin, the most significant structural differences are in the positions of atoms close to the iron center, as the result of increased iron-to-sulfur bond distances (average of 0.04 Å) and decreased amide proton-to-sulfur H-bond distances (average of 0.09 Å) upon reduction.[12] Molecular dynamics simulations also predict that the structural differences between the oxidized and reduced forms of Rdx are localized to the region surrounding the Fe−S center.[13]

The unpaired electron spin density in paramagnetic proteins such as Rdx exhibits strong (hyperfine) interactions with nearby NMR-active nuclei. These strong interactions are manifested by large perturbations in chemical shifts of the nuclei and by efficient relaxation mechanisms that broaden signals and interfere with conventional coherence transfer experiments. Although they pose serious impediments to the standard approaches to protein structure determination in solution by NMR spectroscopy, which are based on pairwise nuclear−nuclear interactions (nuclear Overhauser effects and spin−spin couplings), the electron−nuclear interactions contain other kinds of information.[14] Through-space, metal-centered, dipolar interactions in proteins have been studied for over 25 years.[15] In heme systems, anisotropic magnetic susceptibility tensors determined experimentally from an analysis of pseudocontact shifts[16] have been used to refine structures on the basis of minimizing calculated and experimental pseudocontact shifts. This approach has been applied to studies of the docking of cytochrome b_5 with cytochrome *c*,[17] refinement of the solution structure of horse heart ferricytochrome *c* by the addition of paramagnetic dipolar constraints,[18] and an investigation of conformational changes in horseradish peroxidase induced by substrate binding.[19] In addition, Bertini et al. have employed both chemical shift (pseudocontact)[20−25] and longitudinal relaxation rates[26] resulting from hyperfine interactions as constraints in protein structure determinations.

A recent approach has been to exploit the partial ordering of molecules in high magnetic fields to gain information on structure and dynamics from residual nuclear dipolar couplings.[27−34] Dipolar couplings report on the magnitude and orientation of the internuclear dipolar vector relative to an internal molecular coordinate system. Initial approaches utilized the inherent tendency of some biomolecules to orient with the magnetic field,[27−31] while subsequent applications utilized liquid crystal media to obtain partial ordering of virtually any sample.[32,33,35−38]

For direct magnetic ordering, the degree of alignment depends on the magnitude of the external field and the anisotropy of the molecular magnetic susceptibility tensor, $\Delta\chi$. As the result of partial alignment, the nuclear−nuclear dipolar couplings no longer average to zero. The magnitudes of the resulting couplings are proportional to the square of the external magnetic field. In the case of a molecule with a known anisotropy but an unknown structure, the set of dipolar couplings can be used to investigate the structure and local dynamics of the molecule.[31] In the case of a rigid molecule with a known structure, the dipolar couplings can be used to determine the magnetic susceptibility anisotropy.[30] In paramagnetic molecules, the magnetic susceptibility anisotropy can be used to calculate the dipolar (pseudocontact) contributions from the paramagnetic center to the observed chemical shifts.[15,16,19,27,39,40]

In this study, we have measured one-bond $^{1}H^{N}-^{15}N$ and $^{1}H^{\alpha}-^{13}C^{\alpha}$ couplings in oxidized and reduced Rdx at multiple

(10) Xia, B.; Wilkens, S. J.; Westler, W. M.; Markley, J. L. *J. Am. Chem. Soc.* **1998**, *120*, 4893−4894.
(11) Wilkens, S. J.; Xia, B.; Volkman, B. F.; Weinhold, F.; Markley, J. L.; Westler, W. M. *J. Phys. Chem. B* **1998**, *102*, 8300−8305.
(12) Day, M. W.; Hsu, B. T.; Joshua-Tor, L.; Park, J.-B.; Zhou, Z. H.; Adams, M. W. W.; Rees, D. C. *Protein Sci.* **1992**, *1*, 1494−1507.
(13) Shenoy, V. S.; Ichiye, T. *Proteins* **1993**, *17*, 152−160.
(14) Bertini, I.; Luchinat, C. *NMR of Paramagnetic Molecules in Biological Systems*; Benjamin/Cummings: Menlo Park, CA, 1986.
(15) Horrocks, W. D.; Greenberg, E. S. *Biochim. Biophys. Acta* **1973**, *332*, 38−44.
(16) Emerson, S. D.; La Mar, G. N. *Biochemistry* **1990**, *29*, 1556−1566.
(17) Guiles, R. D.; Sarma, S.; Digate, R. J.; Banville, D.; Basus, V. J.; Kuntz, I. D.; Waskell, L. *Nat. Struct. Biol.* **1996**, *3*, 333−339.
(18) Qi, P. X. R.; Beckman, R. A.; Wand, A. J. *Biochemistry* **1996**, *35*, 12275−12286.
(19) DeRopp, J. S.; Mandal, P.; Brauer, S. L.; La Mar, G. N. *J. Am. Chem. Soc.* **1997**, *119*, 4732−4739.
(20) Banci, L.; Bertini, I.; Delarosa, M. A.; Koulougliotis, D.; Navarro, J. A.; Walter, O. *Biochemistry* **1998**, *37*, 4831−4843.
(21) Arnesano, F.; Banci, L.; Bertini, I.; Felli, I. C. *Biochemistry* **1998**, *37*, 173−184.
(22) Assfalg, M.; Banci, L.; Bertini, I.; Bruschi, M.; Turano, P. *Eur. J. Biochem.* **1998**, *256*, 261−270.
(23) Banci, L.; Bertini, I.; Bren, K. L.; Cremonini, M. A.; Gray, H. B.; Luchinat, C.; Turano, P. *J. Biol. Inorg. Chem.* **1996**, *1*, 117−126.
(24) Banci, L.; Bertini, I.; Savellini, G. G.; Romagnoli, A.; Turano, P.; Cremonini, M. A.; Luchinat, C.; Gray, H. B. *Proteins* **1997**, *29*, 68−76.
(25) Banci, L.; Bertini, I.; Gray, H. B.; Luchinat, C.; Reddig, T.; Rosato, A.; Turano, P. *Biochemistry* **1997**, *36*, 9867−9877.
(26) Bentrop, D.; Bertini, I.; Cremonini, M. A.; Forsen, S.; Luchinat, C.; Malmendal, A. *Biochemistry* **1997**, *36*, 11605−11618.
(27) Tolman, J. R.; Flanagan, J. M.; Kennedy, M. A.; Prestegard, J. H. *Proc. Natl. Acad. Sci. U.S.A.* **1995**, *92*, 9279−9283.
(28) Kung, H. C.; Wang, K. Y.; Goljer, I.; Bolton, P. H. *J. Magn. Reson. B* **1995**, *109*, 323−325.
(29) Tjandra, N.; Omichinski, J. G.; Gronenborn, A. M.; Clore, G. M.; Bax, A. *Nat. Struct. Biol.* **1997**, *4*, 732−738.
(30) Tjandra, N.; Grzesiek, S.; Bax, A. *J. Am. Chem. Soc.* **1996**, *118*, 6264−6272.
(31) Tolman, J. R.; Flanagan, J. M.; Kennedy, M. A.; Prestegard, J. H. *Nat. Struct. Biol.* **1997**, *4*, 292−297.
(32) Tjandra, N.; Bax, A. *Science* **1997**, *278*, 1111−1114.
(33) Tjandra, N.; Bax, A. *J. Biomol. NMR* **1997**, *10*, 289−292.
(34) Banci, L.; Bertini, I.; Huber, J. G.; Luchinat, C.; Rosato, A. *J. Am. Chem. Soc.* **1998**, *120*, 12903−12909.
(35) Hansen, M. R.; Rance, M.; Pardi, A. *J. Am. Chem. Soc.* **1998**, *120*, 11210−11211.
(36) Ottiger, M.; Bax, A. *J. Biomol. NMR* **1998**, *12*, 361−372.
(37) Wang, H.; Eberstadt, M.; Olejniczak, E. T.; Meadows, R. P. *J. Biomol. NMR* **1998**, *12*, 443−446.
(38) Losonczi, J. A.; Prestegard, J. H. *J. Biomol. NMR* **1998**, *12*, 447−451.
(39) Jesson, J. P. In *NMR of Paramagnetic Molecules: Principles and Applications*; La Mar, G. N., Horrocks, W. D., Holm, R. H., Eds.; Academic Press: New York/London, 1973; pp 2−51.
(40) Kurland, R. J.; McGarvey, B. R. *J. Magn. Reson.* **1970**, *2*, 286−301.

magnetic field strengths. This has enabled the decomposition of these couplings into their scalar and dipolar components. The dipolar couplings have been analyzed in terms of the three structural models for Fe(III) Rdx determined by X-ray crystallography and available from the Protein Data Bank to yield the magnetic susceptibility anisotropies. The fitted values for magnetic susceptibility anisotropies were then used to predict pseudocontact contributions to ^{1}H chemical shifts of both oxidation states for comparison with the observed chemical shift differences. The results indicate that, for residues distant enough from the iron center in Rdx not to experience significant contact interactions or broadening, the redox-dependent chemical shift differences can be explained adequately by electron−nuclear dipolar effects (oxidation-state-dependent differences in pseudocontact shifts) without any need to postulate conformational differences.

Experimental Procedures

Sample Preparation. Previously published procedures[6] were used for the heterologous production from *Escherichia coli* of samples of *Clostridium pasteurianum* rubredoxin (Rdx) labeled uniformly with ^{15}N and ^{13}C. The apoprotein was purified and reconstituted with iron to yield Fe(III) Rdx. Solutions of oxidized rubredoxin were reduced by adding excess solid sodium dithionite. All experiments discussed below were performed on 5 mM protein samples in 100 mM potassium phosphate buffer with 100 mM KCl at pH 5.0. The isotopic composition of the solvent was 90% H_2O/10% D_2O in all samples, except for oxidized ^{13}C-labeled Rdx, where it was 99.9% D_2O.

NMR Spectroscopy. All NMR spectra were recorded at 10 °C on Bruker DMX750, DMX600, and DMX400 spectrometers equipped with ^{1}H/^{15}N/^{13}C or ^{1}H/^{15}N/^{13}C/^{31}P probes and *Z*- or three-axis pulsed field gradient capabilities. Quadrature detection in the indirectly detected dimensions was obtained with the States-TPPI method.[41] Each set of *J*-modulated heteronuclear single quantum coherence (HSQC) data was collected twice as a means of estimating experimental uncertainties.

A quantitative *J*-modulated ^{15}N HSQC experiment[30] was used to obtain one-bond ^{1}H−^{15}N couplings at 400, 600, and 750 MHz for oxidized and reduced Rdx. All spectra were acquired with 16 scans per FID, 128 complex ^{15}N points, and 512 complex ^{1}H points. Spectral widths at 750, 600, and 400 MHz were 10 000, 10 000, and 6250 Hz for ^{1}H and 2500, 2000, and 1333.33 Hz for ^{15}N. Series of 2D spectra were obtained at each field strength with 10 different values for the *J*-modulation period 2Δ: 45.3, 46.1, 47.5, 48.9, 50.3, 56.5, 57.4, 58.3, 59.9, and 61.0 ms.

A quantitative *J*-modulated ^{13}C CT-HSQC experiment[42] was used to obtain one-bond ^{1}H−^{13}C couplings at 400 and 750 MHz for oxidized and reduced Rdx. All spectra were acquired with 16 scans per FID, 128 complex ^{13}C points, and 512 complex ^{1}H points. Spectral widths at 750 and 400 MHz were 8333.33 and 5000 Hz for ^{1}H and 6250 and 4000 Hz for ^{13}C. A series of 2D spectra were obtained at each field strength with 10 different values of the *J*-modulation period $2T - 2\Delta$: 23.2, 23.6, 24.0, 24.4 24.8, 25.2, 25.6, 26.0, 26.4, and 28.0 ms.

All Fourier transformations of NMR data were performed with Felix 95.0 (Molecular Simulations, San Diego, CA). Time domain data in both dimensions were apodized with a 75° squared, shifted sine bell function and zero-filled to a final data size of 1024 (^{1}H) × 512 (^{15}N or ^{13}C). The initial value of the incremented delay in each experiment was calculated to produce a −180° first-order phase correction and a flat baseline in the indirect dimension.[43] All ^{1}H dimensions were referenced to internal 2,2-dimethyl-2-silapentane-5-sulfonate (DSS). Indirect ^{13}C and ^{15}N dimensions were referenced indirectly to DSS as previously described.[44] Complete ^{1}H, ^{15}N, and ^{13}C resonance assignments of non-hyperfine-shifted signals were obtained previously for oxidized and reduced Rdx (BioMagResBank accession numbers 4050 and 4051, respectively).[7,8]

Determination of One-Bond Couplings. The peak intensities of resolved signals in the ^{1}H−^{15}N and ^{1}H−^{13}C 2D spectra were measured with a suite of Felix macros and scripts written by Dr. Mikael Akke. Uncertainties in peak intensities were estimated from duplicate measurements. The Levenberg−Marquardt method was used to obtain values of $^1J_{NH}$ by fitting peak intensities and the corresponding dephasing delays (2Δ) to the relation

$$I(2\Delta) = A[C + \cos(2\pi^1 J_{NH}\Delta)] \exp(-2\Delta/T_2^*) \quad (1)$$

where A is the initial amplitude of the signal, T_2^* is the apparent ^{15}N transverse relaxation time, and C accounts for incomplete inversion of ^{1}H magnetization due to pulse imperfection. Similarly, the values of $^1J_{C\alpha H\alpha}$ were obtained from fits to the function

$$I(2T - 2\Delta) = A \cos[2\pi^1 J_{C\alpha H\alpha}(T - \Delta)] \quad (2)$$

where $2T - 2\Delta$ was the dephasing delay.

Determination of $\Delta\chi_{ax}$ and $\Delta\chi_{rh}$ for Rdx. The dipolar couplings were derived by decomposing the experimental values obtained at 400 and 750 MHz (^{1}H frequency): $^1D_{NH} = {}^1J_{NH}(750) - {}^1J_{NH}(400)$; $^1D_{C\alpha H\alpha} = {}^1J_{C\alpha H\alpha}(750) - {}^1J_{C\alpha H\alpha}(400)$. The observed dipolar coupling ($^1D_{HX}$) can be described in terms of the magnitudes of the axial ($\Delta\chi_{ax}$) and rhombic ($\Delta\chi_{rh}$) components of the magnetic susceptibility tensor and the Euler angles α, β, and γ defining its orientation relative to the Cartesian coordinate frame of the crystal structure. The expression used to calculate dipolar couplings for a given magnetic susceptibility anisotropy ($\Delta\chi_{ax}$ and $\Delta\chi_{rh}$) is

$$^1D_{HX} = C\left[\Delta\chi_{ax}(3\cos^2\theta - 1) + \frac{3}{2}\Delta\chi_{rh}(\sin^2\theta\cos 2\phi)\right] \quad (3)$$

where spherical polar coordinates θ and ϕ define the orientation of the internuclear dipolar vector in the coordinate system of the susceptibility tensor (defined by α, β, and γ) and C contains the dependence on the nuclear magnetogyric ratios, the internuclear distance, and the difference between the squares of the two static magnetic fields, $[B_0(750)^2 - B_0(400)^2]$.[27] The software routine MALIGN, written in-house in FORTRAN-77, which takes as input data the list of dipolar couplings with the appropriate residue number and a coordinate file in PDB format, was used to solve for $\Delta\chi_{ax}$, $\Delta\chi_{rh}$, α, β, and γ.[30,45]

To analyze the NMR data in terms of the three available X-ray structures for Rdx (PDB entries 1IRO, 4RXN, and 5RXN), the two other coordinate sets were superimposed on that for 1IRO to obtain a common reference frame for the subsequent calculations. For each of the six sets of input data (NH, CH, and NH + CH dipolar couplings for oxidized and reduced Rdx) and each of the three X-ray structures, a five-dimensional grid search was performed, followed by Powell minimization starting from the global minimum identified in the grid search. A series of 150 Monte Carlo simulations was then performed, from which uncertainties in the fitted values were obtained. An estimate of the diamagnetic contribution to the magnetic susceptibility anisotropy of Rdx was calculated from each of the three X-ray structures by summing the $\Delta\chi_{ax}$ and $\Delta\chi_{rh}$ values of the aromatic and peptide groups.[30]

Pseudocontact Shift Calculations. Pseudocontact shifts were calculated for the backbone protons of rubredoxin from the three X-ray structures of oxidized Rdx and the experimentally determined magnetic susceptibility anisotropy values for oxidized and reduced Rdx. The pseudocontact shift in the absence of significant zero-field splitting is described by the expression

$$\Delta pc = -\frac{1}{3r^3}\left[\Delta\chi_{ax}(3\cos^2\theta - 1) + \frac{3}{2}\Delta\chi_{rh}(\sin^2\theta\cos 2\phi)\right] \quad (4)$$

(41) Marion, D.; Wüthrich, K. *Biochem. Biophys. Res. Commun.* **1983**, *113*, 967−974.
(42) Tjandra, N.; Bax, A. *J. Magn. Reson.* **1997**, *124*, 512−515.
(43) Bax, A.; Ikura, M.; Kay, L. E.; Zhu, G. *J. Magn. Reson.* **1991**, *91*, 174−178.
(44) Wishart, D. S.; Bigam, C. G.; Yao, J.; Abildgaard, F.; Dyson, H. J.; Oldfield, E.; Markley, J. L.; Sykes, B. D. *J. Biomol. NMR* **1995**, *6*, 135−140.
(45) Abragam, A.*The Principles of Nuclear Magnetism*; Oxford University Press: Oxford, 1961;

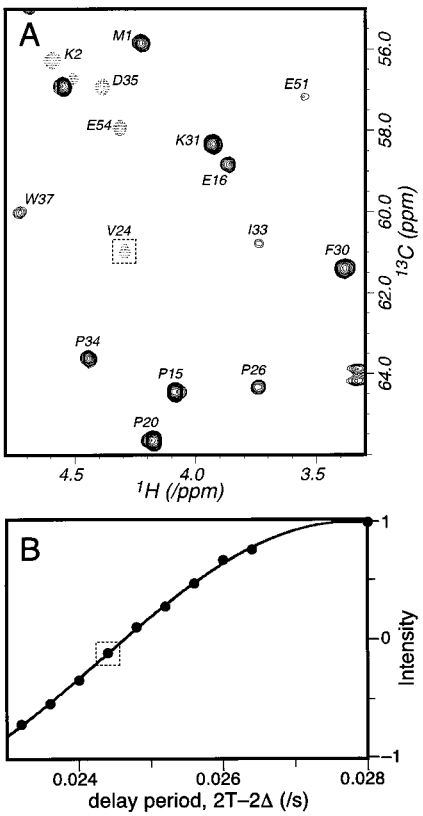

Figure 1. (A) Portion of the 750-MHz 2D $^{1}J_{C\alpha H\alpha}$-modulated $^{13}C-^{1}H$ CT-HSQC spectrum of Fe(II) Rdx, recorded with a total dephasing delay of 24.4 ms. Dotted contours represent negative intensity, and the signal corresponding to Val[24] is boxed. (B) The intensity of the signal from Val[24] is plotted as a function of the total dephasing delay, and the point corresponding to the spectrum shown in (A) is boxed.

where r, θ, and ϕ describe the position of the nucleus in the axis system of the magnetic susceptibility tensor and $\Delta\chi_{ax}$ and $\Delta\chi_{rh}$ are its axial and rhombic components.[40] Because the values for $\Delta\chi_{ax}$ and $\Delta\chi_{rh}$ obtained from fits to dipolar couplings reflect the contributions of both the paramagnetic and diamagnetic susceptibility anisotropies of Rdx, pseudocontact shifts calculated in this manner will not accurately predict the true values of Δpc for the oxidized or reduced Rdx species individually. However, if the backbone and aromatic side chains of Rdx are not significantly displaced, subtracting the Δpc values calculated for the two oxidation states will remove the contribution from the diamagnetic susceptibility anisotropy. This calculated chemical shift difference may then be compared directly with the observed chemical shift differences between oxidized and reduced Rdx.

Results and Discussion

Field Dependence of $^{1}J_{NH}$ and $^{1}J_{C\alpha H\alpha}$ Splittings. One-bond $^{15}N-^{1}H^{N}$ splittings were measured at 400, 600, and 750 MHz, and $^{13}C^{\alpha}-^{1}H^{\alpha}$ splittings were measured at 400 and 750 MHz. A portion of one $^{13}C^{\alpha}-^{1}H^{\alpha}$ spectrum is shown in Figure 1, along with an example of a fit of peak intensities. Figure 2 contains a summary of the field-dependent contribution to $^{1}J_{NH}$ and $^{1}J_{C\alpha H\alpha}$ for both oxidized and reduced Rdx, obtained from the difference between the splittings obtained at 750 and 400 MHz. A clear field dependence was observed for both oxidized and reduced Rdx, with the 750−400 difference 2-fold larger than the 600−400 difference (data not shown), as expected from the dependence on the square of the field strength. In addition, the field-dependent contributions are significantly larger for the reduced form (Figure 2A) than for the oxidized form (Figure 2B) of Rdx.

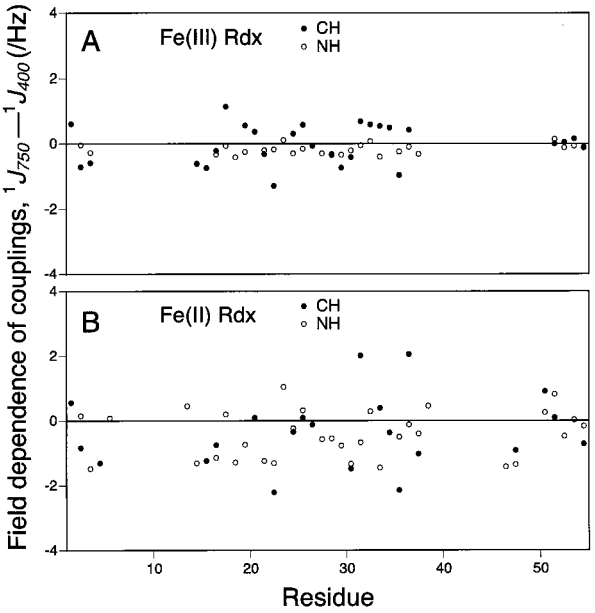

Figure 2. Summary of field-dependent splittings measured for rubredoxin, plotted as a function of residues number. C−H and N−H splittings are shown as filled and open circles, respectively. (A) Field-dependent splittings for Fe(III) Rdx. (B) Field-dependent splittings for Fe(II) Rdx.

Magnetic Susceptibility Anisotropy from $^{1}D_{NH}$ and $^{1}D_{C\alpha H\alpha}$ Splittings. The axial and rhombic components of the magnetic susceptibility tensor, $\Delta\chi_{ax}$ and $\Delta\chi_{rh}$, and the Euler angles α, β, and γ, which describe its orientation in the coordinate frame of the crystal structure, were obtained from minimization of the difference between the observed and predicted splittings, as described by Tjandra et al.[30] The global minimum for this function was found with a five-dimensional grid search followed by Powell minimization. Uncertainties in the fitted parameters were estimated from Monte Carlo simulations. The $^{1}D_{NH}$ and $^{1}D_{C\alpha H\alpha}$ splittings were analyzed separately and in combination for both the oxidized and reduced forms of Rdx. Initial analysis of the $^{1}D_{NH}$ splittings used a six-parameter fit, which included a constant to account for the possible contribution of cross-correlation effects (the dynamic frequency shift, or DFS) to the field dependence of $^{1}J_{NH}$ values.[30] For both oxidized and reduced Rdx, a value of −0.12 Hz was obtained for the DFS contribution to the difference in $^{1}J_{NH}$ between 400 and 750 MHz. A similar test was applied to the $^{1}D_{C\alpha H\alpha}$ splittings, but as expected,[42] a negligible DFS contribution was obtained. After the DFS contribution was subtracted out, the $^{1}D_{NH}$ values were scaled up by a factor of 2.09 to account for the different magnetogyric ratios and H−X bond lengths of ^{15}N and ^{13}C (using 1.02 and 1.08 Å, respectively). The combined $^{1}D_{C\alpha H\alpha}$ and scaled $^{1}D_{NH}$ splittings were then fitted simultaneously to each Rdx structure. Examples of the fitting results are shown in Figure 3. Cross-correlation between Curie spin−nuclear dipole and nuclear dipole−nuclear interactions has been shown to be another possible source for DFS.[46] However, calculations for both oxidized and reduced Rdx indicated that this interaction did not contribute significantly to the observed dipolar couplings; thus, this effect was ignored in the analysis.

A unique, best-fit orientation of the susceptibility tensor for Fe(II) Rdx is clearly identified in Figure 3A, which shows the reduced error, E_v, as a function of the Euler angles, α and β. Another way to evaluate the degree to which a set of data is

(46) Ghose, R.; Prestegard, J. H. *J. Magn. Reson.* **1997**, *128*, 138−143.

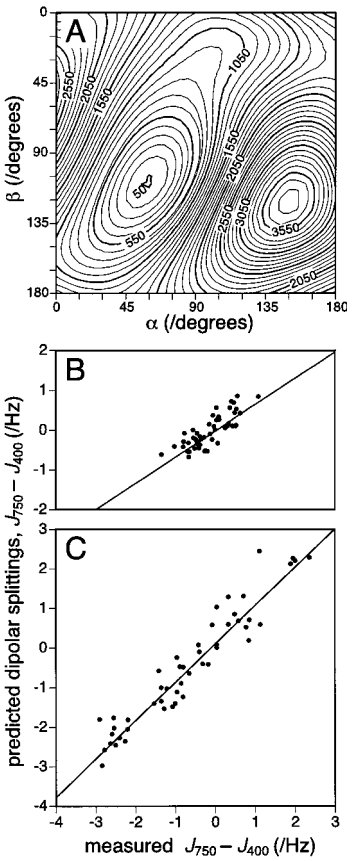

Figure 3. Fitting of the experimental dipolar splittings to the crystal structures of *Clostridium pasteurianum* Rdx. (A) Contour plot based on the results of a five-dimensional grid search to find the values of $\Delta\chi_{ax}$, $\Delta\chi_{rh}$, α, β, and γ, which minimize the difference between the measured $^1H-^{15}N$ and $^1H-^{13}C$ dipolar couplings ($^1D_{NH}$) for reduced Rdx and those calculated from the 5RXN structure of oxidized Rdx and the fitted parameters. The reduced error, E_v, is shown as a function of α and β. Correlations between measured and calculated dipolar couplings ($^1D_{NH}$ and $^1D_{C\alpha H\alpha}$) are shown for (B) oxidized and (C) reduced Rdx. The calculated values are based on the fitted susceptibility tensor parameters shown in Table 1 for the 5RXN structure and the combined NH and CH data. Before simultaneous fitting of N−H and C−H splittings to the structures, −0.12 Hz was subtracted from the experimental N−H splittings to account for the field-dependent contribution of the dynamic frequency shift (DFS). The corrected N−H splittings were then multiplied by a factor of −2.0904 to account for the ratio of the magnetogyric ratios of ^{13}C and ^{15}N as well as the difference in $^1H-^{15}N$ and $^1H-^{13}C$ bond lengths. The linear least-squares best fit is shown for each plot. For oxidized Rdx, a slope of 0.66 and *y*-intercept of −0.004 were obtained from this fit, with a correlation coefficient (R^2) of 0.66. For the reduced protein, a slope of 0.97 and *y*-intercept of 0.01 were obtained, with a correlation coefficient (R^2) of 0.91.

consistent with a single set of susceptibility anisotropy parameters is to plot the experimental splittings versus splittings calculated from the fitted parameters. Such correlation plots for fits of the combined NH and CH data to the 5RXN crystal structure are shown in Figure 3B,C for oxidized and reduced Rdx, respectively. All six combinations of dipolar splitting data were fitted to the three high-resolution X-ray structures of Rdx available from the Protein Data Bank. The results are summarized in Table 1. Also shown in Table 1 are the nonparamagnetic contributions to the magnetic susceptibility anisotropy from aromatic and peptide bonds, as calculated from each of the three crystal structures of Rdx.[2−4]

The measured magnetic susceptibility anisotropy of reduced

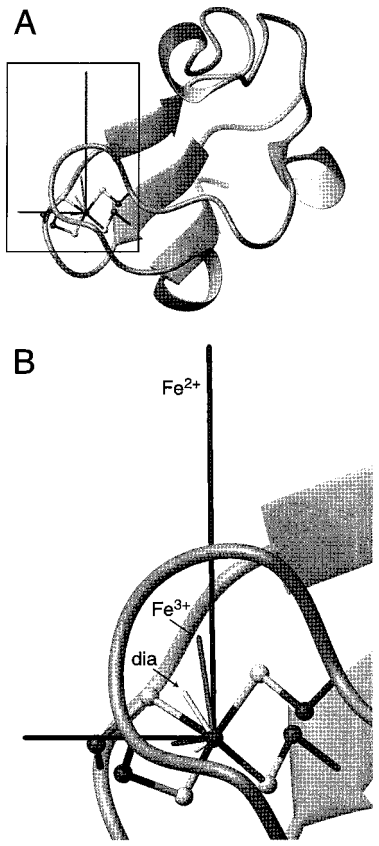

Figure 4. Structural representation of magnetic susceptibility anisotropies. A ribbon diagram of the structure of rubredoxin is shown, including the atoms of the FeS_4 cluster. Vectors originating at the iron indicate the magnitudes and show the orientations of the $\Delta\chi_{ax}$ and $\Delta\chi_{rh}$ terms obtained from fits to the 5RXN structure of dipolar splittings from iron(II) (Fe^{2+}) and iron(III) (Fe^{3+}) rubredoxin. The diamagnetic $\Delta\chi_{ax}$ and $\Delta\chi_{rh}$ values calculated for 5RXN are also shown (dia).

($S = 2$) Rdx is nearly 4 times that of oxidized ($S = {}^5/_2$) Rdx, as evident from the significantly larger splittings (Figure 2). The magnitudes and orientations of the measured $\Delta\chi$ values relative to the 5RXN structure of Rdx are illustrated in Figure 4. The susceptibility tensor was better defined for Fe(II) Rdx, where the values derived for all three sets of input data (NH, CH, and NH + CH) were similar, than for Fe(III) Rdx, where the fitted parameters varied somewhat with the input data. An indication of the reliability of the fitted parameters comes from a comparison of the reduced errors obtained from the five-parameter fits (E_v) with the reduced error for a model with zero magnetic susceptibility anisotropy [$E_v(0)$]. A reduction in E_v of ∼10-fold was obtained for reduced Rdx by fitting to a nonzero anisotropy, while the $E_v(0)$-to-E_v ratio for oxidized Rdx was much smaller. This is due, in part, to an apparent discrepancy between the NH and CH splittings, which individually appeared to produce good fits but,when combined, led to only a 2-fold reduction in the reduced error. The difference most likely stems from the greater relative uncertainty in the measured dipolar couplings for Fe(III) Rdx than for Fe(II) Rdx.

Fits to the individual NH and CH data sets for reduced Rdx produced susceptibility tensor orientations that agreed very well with that obtained from the combined NH and CH splittings, but magnitudes ($\Delta\chi_{ax}$ and $\Delta\chi_{rh}$) of the susceptibility anisotropy obtained from the NH and CH data differed by ∼25%. Disagreement between the magnitudes of the susceptibility tensors for Fe(II) Rdx derived from the NH and CH dipolar couplings may reflect differences in the vibrational and libra-

Table 1. Magnetic Susceptibility Anisotropies for Reduced and Oxidized *Clostridium pasteurianum* Rubredoxin at 10 °C

		$\Delta\chi$, 10^{-28} cm^3/molecule						
	PDB[a]	$\Delta\chi_{ax}$	$\Delta\chi_{rh}$	α^b(deg)	β^b (deg)	γ^b (deg)	$E_v{}^c$	$E_v(0)^d$
				Reduced Rdx				
NH	1IRO	21.3 ± 0.16[e]	9.71 ± 0.14	59.2 ± 0.2	108.6 ± 0.3	142.8 ± 0.5	47 ± 3	
	4RXN	20.7 ± 0.17	9.78 ± 0.14	58.4 ± 0.2	108.0 ± 0.3	144.5 ± 0.5	73 ± 3	821
	5RXN	22.1 ± 0.17	9.55 ± 0.14	58.4 ± 0.2	108.4 ± 0.3	142.0 ± 0.5	53 ± 3	
CH	1IRO	17.5 ± 0.28	8.7 ± 0.19	59.2 ± 0.4	106.6 ± 0.4	144.3 ± 0.8	38 ± 3	
	4RXN	13.0 ± 0.20	8.6 ± 0.19	48.2 ± 0.7	115.5 ± 0.8	144.6 ± 0.7	60 ± 4	402
	5RXN	17.9 ± 0.29	9.9 ± 0.20	58.6 ± 0.4	112.2 ± 0.5	150.1 ± 0.6	39 ± 3	
NH + CH	1IRO	19.8 ± 0.15	9.4 ± 0.11	59.9 ± 0.2	107.0 ± 0.3	145.0 ± 0.4	43 ± 2	
	4RXN	17.9 ± 0.13	9.2 ± 0.12	57.2 ± 0.2	107.9 ± 0.3	147.4 ± 0.4	81 ± 2	659
	5RXN	20.3 ± 0.14	9.7 ± 0.11	59.2 ± 0.2	109.0 ± 0.3	146.6 ± 0.4	52 ± 2	
				Oxidized Rdx				
NH	1IRO	5.27 ± 0.17	0.19 ± 0.50	66.2 ± 1.0	111.8 ± 1.1	229 ± 73	5.1 ± 1.0	
	4RXN	5.70 ± 0.20	0.79 ± 0.18	63.2 ± 0.9	114.3 ± 1.1	121 ± 7	4.7 ± 0.9	35.44
	5RXN	4.93 ± 0.17	0.22 ± 0.38	66.4 ± 1.0	108.9 ± 1.2	293 ± 127	7.5 ± 1.2	
CH	1IRO	6.78 ± 0.18	5.07 ± 0.17	62.1 ± 0.6	94.0 ± 1.0	144.2 ± 1.2	13.5 ± 1.7	
	4RXN	5.43 ± 0.20	5.53 ± 0.18	60.7 ± 0.9	90.5 ± 1.6	148.0 ± 0.9	26.9 ± 2.2	101.36
	5RXN	6.02 ± 0.16	4.81 ± 0.17	61.1 ± 0.7	94.1 ± 1.2	145.2 ± 1.2	18.0 ± 1.9	
NH + CH	1IRO	5.46 ± 0.12	2.27 ± 0.11	62.2 ± 0.6	100.6 ± 0.9	141.6 ± 1.7	27.3 ± 1.5	
	4RXN	4.82 ± 0.13	2.54 ± 0.11	60.7 ± 0.6	102.9 ± 1.1	148.1 ± 1.3	32.7 ± 1.7	69.71
	5RXN	5.28 ± 0.11	2.09 ± 0.11	61.6 ± 0.6	101.2 ± 0.9	144.4 ± 1.8	27.1 ± 1.5	
				Diamagnetic[f]				
	1IRO	−2.98	−1.21	57.0	59.4	149.0		
	4RXN	−3.00	−1.35	73.3	68.8	158.0		
	5RXN	−2.84	−1.10	64.7	72.4	152.9		

[a] Each set of dipolar couplings (NH, CH, and combined) for both oxidized and reduced Rdx was fitted to the three high-resolution X-ray structures available for oxidized *C. pasteurianum* rubredoxin, identified by PDB accession code. [b] Euler angles in the frame of the 1IRO PDB coordinates of rubredoxin. [c] Reduced error calculated assuming uncertainties of 0.03 and 0.06 Hz for ^{1}H−^{15}N and ^{1}H−^{13}C dipolar couplings, respectively. [d] Reduced error calculated for zero magnetic susceptibility anisotropy. [e] Uncertainties derived from standard deviations of fitted parameters in 150 Monte Carlo simulations. [f] Contributions to the magnetic susceptibility anisotropy from aromatic and peptide groups, calculated from the X-ray structures.

tional dynamics of the two types of bonds. Recent dipolar coupling measurements by Ottiger and Bax suggest these motions result in effective backbone NH and CH bond lengths of 1.041 and 1.117 Å, respectively.[47] However, substitution of these values in the determination of the susceptibility anisotropy parameters in Table 1 produced only a 5% change in the scaling factor for NH and CH couplings; this refinement removed only 6% of the 25% discrepancy.

The diamagnetic susceptibility anisotropies calculated from the three X-ray structures of Fe(III) Rdx (Table 1) are similar to that measured for ubiquitin[30] and are roughly equivalent to the combined contribution of three phenylalanine side chains [$\Delta\chi_{ax}$(Phe) = -1.0×10^{-28}]. The magnitudes of the axial and rhombic components of the calculated diamagnetic susceptibility anisotropy are about one-half those of Fe(III) Rdx and about one-seventh those of Fe(II) Rdx. The relatively larger contribution of the diamagnetic component to the magnetic susceptibility anisotropy of Fe(III) Rdx than to that of Fe(II) Rdx accounts for part of the divergence of the $\Delta\chi_{ax}$ vectors (Figure 4).

Pseudocontact Shift Calculations. Chemical shift differences between oxidized and reduced Rdx have been reported for nuclei that are outside the range of Fermi contact interactions (>11 Å from the iron); these shift differences were tentatively ascribed to subtle structural rearrangements.[7,8] However, the influence of pseudocontact origin for these shifts could not be ruled out. Measurement of the magnetic susceptibility anisotropies for these two species now permits us to resolve this issue.

The previously reported differences in ^{1}H$^\alpha$ and ^{1}H^N chemical shifts for oxidized and reduced Rdx are plotted as a function of residue number in Figure 5A. Residues less than ~11 Å [8.5 Å] from the Fe(III) [Fe(II)] experience significant line broadening and could not be assigned using standard 2D and 3D heteronuclear methods. This accounts for the lack of comparative data for residues 5−13 and 38−50. The magnitudes and orientations for $\Delta\chi_{ax}$ and $\Delta\chi_{rh}$ obtained by analysis of dipolar

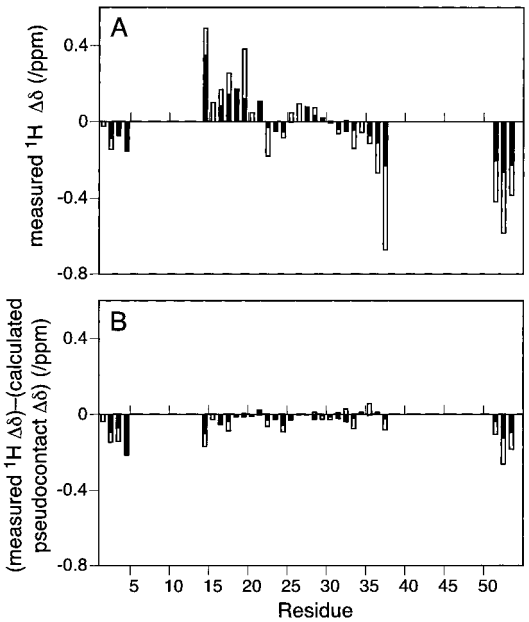

Figure 5. Pseudocontact contributions to ^{1}H chemical shift differences between oxidized and reduced rubredoxin at 10 °C. (A) Differences between ^{1}H$^\alpha$ and ^{1}H^N shifts calculated as (oxidized − reduced). (B) Chemical shift differences after subtraction of calculated pseudocontact shift differences. Pseudocontact shifts were calculated for the 5RXN coordinates using the parameters for magnetic susceptibility anisotropy obtained from fits of ^{1}H−^{15}N and ^{1}H−^{13}C dipolar couplings to the 5RXN structure. The magnitude of the fitted susceptibility tensor was scaled to account for attenuation in the measured value of the magnetic susceptibility anisotropy due to internal motion by assuming an S^2 = 0.85 for all NH and CH bond vectors (S = 0.922). Black and white bars represent ^{1}H^N and ^{1}H$^\alpha$ shift differences, respectively.

(47) Ottiger, R.; Bax, A. *J. Am. Chem. Soc.* **1998**, *120*, 12334−12341.

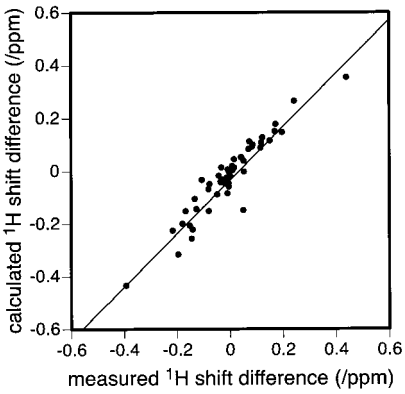

Figure 6. Correlation between calculated pseudocontact shift differences and observed shift differences determined using the 5RXN structure of rubredoxin. Solid line represents the best linear fit to the data, with a slope of 1.01, intercept of −0.035, and $R^2 = 0.89$.

splittings were used to calculate pseudocontact shifts for oxidized and reduced Rdx according to eq 4 for each of the three crystal structures. The difference between calculated pseudocontact shifts for each backbone ^{1}H (oxidized − reduced) was then subtracted from the measured chemical shift differences of Figure 5A. Figure 5B shows the "pseudocontact-corrected" shift differences for oxidized and reduced Rdx. Most of the observed shift differences are removed by this correction, and the differences that remain are within the uncertainties in the corrected shift differences. This indicates that the differential magnetic susceptibility anisotropies of oxidized and reduced Rdx provide the major shift mechanism and that the shift differences provide no evidence for conformational differences in these regions of the protein. In another representation of this result (Figure 6), a strong correlation is found between the experimental shift differences and those calculated from the magnetic susceptibility anisotropies.

Summary and Implications for Structural Analysis of Paramagnetic Proteins. Precise values for the backbone one-bond ^{15}N−^{1}H and $^{13}C^{\alpha}$−$^1H^{\alpha}$ splittings of Rdx in both its Fe(II) and Fe(III) states have been obtained at multiple magnetic field strengths. The field-dependent components of these splittings arise from dipolar couplings that are incompletely averaged by molecular reorientation in solution. Because the magnetic susceptibility anisotropy of Rdx is dominated by the iron center, the degree of magnetic alignment responsible for the observed dipolar couplings is different for the two oxidation states of Rdx. Reduced Rdx has a much larger magnetic susceptibility anisotropy than oxidized Rdx; this is evident from the relative magnitudes of the observed dipolar splittings (Figure 2). Analysis of the large number of dipolar couplings in terms of the three-dimensional structure of Fe(III) Rdx (Figure 3) made it possible to determine the magnitude and orientation of the magnetic susceptibility anisotropy for the two oxidation states of Rdx (Figure 4). In analyzing the NMR data for Fe(II) Rdx, the tentative assumption was made that the conformations of the oxidized and reduced forms of the protein are very similar at distances >11 Å from the iron. This assumption was validated when the pseudocontact shift differences calculated for Fe(III) Rdx and Fe(II) Rdx from the susceptibility anisotropies accounted fully for the previously reported[7] chemical shift differences for backbone ^{1}H signals in the diamagnetic spectral region (Figure 6). Thus, these chemical shift differences arise from the change in the anisotropy of the magnetic susceptibility, rather than from a change in the conformation of the protein.

To our knowledge, this study represents the first experimental determinations of the magnetic susceptibility anisotropy and pseudocontact shifts for an oxidized and reduced non-heme iron protein. The results have made it possible to evaluate the pseudocontact contributions to the chemical shifts of both oxidized and reduced Rdx. This has enabled us to reevaluate the pseudocontact contributions to the large hyperfine shifts of oxidized and reduced Rdx that have been analyzed elsewhere.[9] The present results confirm the prior assumption that these shifts are dominated by Fermi contact effects and have negligible pseudocontact contributions.[9] Correction of the experimental chemical shifts of these hyperfine signals for the minor pseudocontact contributions determined here did not affect in a significant way their correlation with calculated Fermi contact spin densities (data not shown). This reinforces the previous conclusion[9] that the much better fit reported between the calculated and observed hyperfine shifts for Fe(III) Rdx than for Fe(II) Rdx arises from small conformational differences in the nuclei that exhibit Fermi contact interactions with the iron (those within ∼7 Å of the iron), which were neglected when the X-ray structure of Fe(III) Rdx was used as the basis for the calculated Fermi contact spin densities of Fe(II) Rdx. Thus, a more comprehensive picture emerges from the combination of NMR results from the hyperfine-shifted signals, which contain evidence for small oxidation-state-dependent structural changes, with those for the diamagnetic region, which indicate that the structure of Rdx >11 Å from the iron remains unchanged. The approaches presented here should be applicable to detailed analysis of electron−nuclear interactions in a wide range of metalloproteins.

Acknowledgment. The authors thank Dr. Nico Tjandra for providing software and helpful discussions and Dr. Ed Mooberry along with other members of the NMRFAM staff for their gracious help. S.J.W. was supported in part by a traineeship from a NIH Molecular Biophysics Training Grant (GM08293). This work was supported in part by NIH Grant GM58667. Equipment in the National Magnetic Resonance Facility at Madison (NMRFAM) was purchased with funds from the University of Wisconsin, the NSF Biological Instrumentation Program (Grant DMB-8415048), NIH Biomedical Research Technology Program (Grant RR02301), NIH Shared Instrumentation Program (Grant RR02781), and the U.S. Department of Agriculture. All data have been deposited in the BioMagResBank at the University of Wisconsin−Madison [BMRB accession numbers 4319 (Fe^{3+} Rdx) and 4320 (Fe^{2+} Rdx)].

JA990079B